11-2014

Heat generation in an elastic binder system with embedded discrete energetic particles due to high-frequency, periodic mechanical excitation

Jesus O. Mares
Purdue University

J K. Miller
Purdue University

I E. Gunduz
Purdue University

J F. Rhoads
Purdue University, jfrhoads@purdue.edu

Steven F. Son
Purdue University, sson@purdue.edu

Recommended Citation
J. O. Mares, J. K. Miller, I. E. Gunduz, J. F. Rhoads, and S. F. Son, "Heat Generation in an Elastic Binder System with Embedded Discrete Energetic Particles due to High-Frequency, Periodic Mechanical Excitation," Journal of Applied Physics, Vol. 116 (20), p. 204902 (2014). dx.doi.org/10.1063/1.4902848

Heat generation in an elastic binder system with embedded discrete energetic particles due to high-frequency, periodic mechanical excitation

J. O. Mares, J. K. Miller, I. E. Gunduz, J. F. Rhoads, and S. F. Son

Citation: Journal of Applied Physics **116**, 204902 (2014);
View online: https://doi.org/10.1063/1.4902848
View Table of Contents: http://aip.scitation.org/toc/jap/116/20
Published by the American Institute of Physics

Heat generation in an elastic binder system with embedded discrete energetic particles due to high-frequency, periodic mechanical excitation

J. O. Mares,[1] J. K. Miller,[2] I. E. Gunduz,[2] J. F. Rhoads,[2] and S. F. Son[2]
[1]*School of Aeronautics and Astronautics, Purdue University, West Lafayette, Indiana 47907, USA*
[2]*School of Mechanical Engineering, Purdue University, West Lafayette, Indiana 47907, USA*

(Received 8 September 2014; accepted 15 November 2014; published online 26 November 2014)

High-frequency mechanical excitation can induce heating within energetic materials and may lead to advances in explosives detection and defeat. In order to examine the nature of this mechanically induced heating, samples of an elastic binder (Sylgard 184) were embedded with inert and energetic particles placed in a fixed spatial pattern and were subsequently excited with an ultrasonic transducer at discrete frequencies from 100 kHz to 20 MHz. The temperature and velocity responses of the sample surfaces suggest that heating due to frictional effects occurred near the particles at excitation frequencies near the transducer resonance of 215 kHz. An analytical solution involving a heat point source was used to estimate heating rates and temperatures at the particle locations in this frequency region. Heating located near the sample surface at frequencies near and above 1 MHz was attributed to viscoelastic effects related to the surface motion of the samples. At elevated excitation parameters near the transducer resonance frequency, embedded particles of ammonium perchlorate and cyclotetramethylene-tetranitramine were driven to chemical decomposition. © *2014 AIP Publishing LLC*. [http://dx.doi.org/10.1063/1.4902848]

I. INTRODUCTION

Prior works have demonstrated that high-frequency mechanical excitation can induce localized heating within many materials.[1–3] The utilization of this phenomenon in composite explosives may lead to the development of novel detection methods,[4] or enhance existing vapor-based trace detection systems by raising the vapor pressures of select high explosives.[5,6] In addition, this excitation could generate stress concentrations and/or hot spots within energetic materials,[7] offering unique pathways for explosives defeat. Despite its potential, the heating of composite energetic materials via high-frequency mechanical excitation remains relatively unexplored. Such excitations are used in the nondestructive testing procedure of vibrothermography to generate heat at locations of voids, delaminations, and inclusions via ultrasonic mechanical excitation. Renshaw *et al.*[8] have classified both friction and viscoelastic losses as major mechanisms associated with heat generation due to this high-frequency excitation. Frictional heating is described as the conversion of mechanical motion into thermal energy due to the interaction between moving interfaces, such as cracks or delaminations. Viscoelastic heating is the process of energy dissipation due to stresses at or near defects, voids, or inclusions and is related to the non-isentropic losses experienced by the material undergoing cyclic motion.[9,10]

Recently, Miller *et al.*[11] and Woods *et al.*[12] have investigated and characterized the heating of a mock energetic composite material (ammonium chloride and hydroxyl-terminated polybutadiene) excited at structural resonances. Their findings illustrate clear, well characterized viscoelastic heating in plastic-bonded mock explosives. The authors also observed that heat generation exceeded the predicted viscoelastic heating responses at high solids loading, suggesting a secondary mechanism attributed to particle interactions. Mares *et al.*[13] have shown evidence of heat generation within an energetic composite material, PBX 9501, excited at frequencies from 50 kHz to 40 MHz. Heating was attributed to both viscoelastic heating of the bulk material, as well as frictional heating due to the motion of the energetic particles within the binder system. Chen *et al.*[14] observed the heating of individual energetic crystals contained within a polymer binder excited by a high-power ultrasonic horn at a frequency of 20 kHz.

Despite these advances, the mechanisms of energy localization due to high-frequency mechanical excitation within a composite explosive system have yet to be fully explored. The objective of this work was to investigate the nature of heating within samples of an elastic binder (Sylgard 184) loaded with five discrete inert and energetic particles of varied material and size under high-frequency, periodic excitation. Samples were excited via ultrasonic transducers from 100 kHz to 20 MHz and the thermal and mechanical responses of the sample surface were measured. Evidence of frictional heating at the particle locations, as well as viscoelastic heating near the sample surface, was observed at select frequencies. Heating rates and temperatures at the particle locations due to frictional heating were estimated. In separate trials utilizing elevated excitation parameters, individual ammonium perchlorate (AP) and cyclotetramethylene-tetranitramine (HMX) particles were driven to chemical decomposition within 15 s, illustrating the effectiveness of this heating method.

II. EXPERIMENTAL PROCEDURES

A. Sample preparation

The tested samples consisted of an elastic binder (Sylgard 184) and five embedded particles, as detailed in Table I. Particles were selected by hand with the use of a

TABLE I. Material properties.

Sample (diameter)	Material	Manufacturer/Supplier
AP (700–850 μm)	Ammonium perchlorate	Firefox Enterprises, Inc.
AP (550–700 μm)	Ammonium perchlorate	Firefox Enterprises, Inc.
AP (400–550 μm)	Ammonium perchlorate	Firefox Enterprises, Inc.
HMX (750–950 μm)	Cyclotetramethylene-tetranitramine	BAE Systems
Sugar (450–600 μm)	Granulated white cane sugar	C&H Sugar Co., Inc.
Steel ball (1580 μm)	1010-1020 Carbon steel	McMaster-Carr Supply Co.
ZS (800–1000 μm)	Zirconium silicate	Union Process, Inc.
ZS (600–800 μm)	Zirconium silicate	Union Process, Inc.
Neat/Binder	Sylgard 184 silicone elastomer	Dow Corning

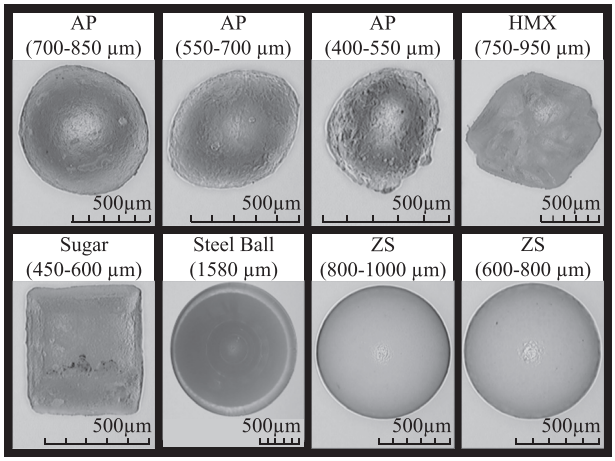

FIG. 1. Images of representative particles used as inclusions in the study.

Hirox KH-8700 digital microscope to fit within the listed diameter ranges. Optical images of representative particles used in each sample are shown in Figure 1. Each sample was produced by molding a 10:1 base to curative mixture of Sylgard 184 into a rectangular block of a nominal height of 2.60 mm with five cavities of a depth of 1.59 mm in a pattern as illustrated in the optical image of the AP (550–700 μm) loaded sample in Figure 2. Particles were individually placed into the cavities and the samples were then covered with Sylgard 184 and molded into a complete rectangular block with a nominal height of 4.00 mm, width of 6.70 mm and length of 9.00 mm. At each step, the samples were degassed at near-vacuum conditions for 10 min and cured at 65 °C for a minimum of 3 h. Steiner & Martins, Inc. SMD10T2R111

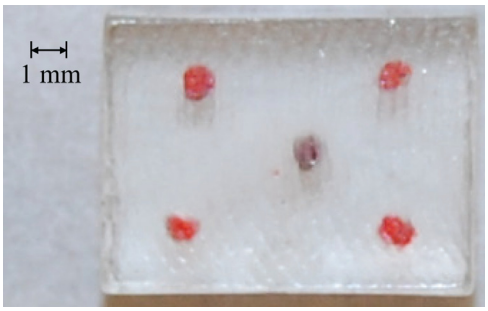

FIG. 2. Optical image of the top side of the AP (700–850 μm) loaded sample. Note the die pattern of the included AP particles, which were dyed in order to increase visual contrast.

piezoelectric ultrasonic transducers were affixed to the bottom side of each sample with Devcon 5 min epoxy and cured at 65 °C for 24 h. The cylindrical transducer is listed as exciting in a "radial" mode and has a center frequency of 215 kHz.

B. Thermal measurements

The aforementioned transducer was excited by a sinusoidal electrical signal supplied by an Agilent N9310A RF signal generator and amplified by a Mini-circuits LZY-22+ amplifier. The supply signal was monitored with the use of a Tektronix DPO 4043 oscilloscope. A schematic diagram of the experimental setup utilized for thermal testing is provided in Figure 3. Each sample was excited at 300 logarithmically spaced frequencies between 100 kHz and 20 MHz, as well as at 100 logarithmically spaced frequencies between 200 kHz and 230 kHz, for 2 s with 10 W of electrical power supplied to the transducer. The surface temperature of the sample at each excitation frequency was measured using a FLIR A325sc thermal camera, which features a maximum frame rate of 30 Hz, temperature sensitivity of 0.07 °C at 30 °C, and accuracy of ±2 °C or ±2% of the reading. To ensure a uniform surface emissivity, the sample was covered with a fine layer of carbon black and an emissivity value of 0.99 was subsequently assumed. The temperature variation due to an emissivity value ranging from 0.95 to 0.99 was less than the listed accuracy of the thermal camera for the temperature ranges reported. The experimental process was automated using a LabVIEW-based system. Once the

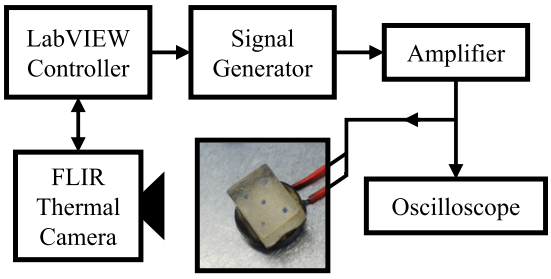

FIG. 3. Schematic of the experimental setup used for the thermal experiments described herein. Note the ultrasonic transducer epoxied to the bottom side of the sugar (450–600 μm) loaded sample. The thermal camera was focused on the top surface of the samples, which were coated in carbon black (not pictured). The sugar particles were dyed in order to increase visual contrast.

excitation and measurement of the sample were completed for a selected frequency, the sample was allowed to reach thermal equilibrium with ambient conditions before proceeding to the next excitation frequency. High-speed optical imaging was performed with a Phantom v7.3 camera operating at 1000 frames per second.

C. Mechanical measurements

A Polytec MSA-400 microscale scanning laser Doppler vibrometer (LDV) was employed to record mechanical-domain responses of all samples in separate trials. The samples were electrically excited by band limited white noise from 100 kHz to 5 MHz at an excitation level of 130 mW. This excitation was supplied to the transducers by the same signal generator and amplifier used in the thermal experiments. The surface velocity was recorded on a discrete grid of points across the sample surface. Through a comparison of the velocity data to the input voltage profiles, linear estimates of the frequency response were calculated at each point. The spatial grid had a density of 35 × 45 points, and the frequency resolution was approximately 200 Hz. At each grid point, 50 individual measurements were averaged. For the purposes of LDV testing, the samples were coated in a reflective silver paint which allowed for improvements in signal return. The very thin layer of silver paint was assumed to be perfectly bonded to the sample surface and comparatively massless. The samples were supported at the transducer interface, allowing for free vibrations of the top surface.

III. RESULTS

The maximum surface temperatures measured at 2 s of excitation for the AP (700–850 μm) loaded and neat samples from 100 to 20 000 kHz are displayed in Figure 4. The surface temperature rises of the samples were significant only at select frequencies. Furthermore, for each sample, the magnitudes of the surface temperature rises were significantly higher at select frequencies near and above 1 MHz than at the peak near the listed transducer center frequency of 215 kHz. All samples exhibited a similar thermal response dependency on excitation frequency except near 215 kHz, at which each thermal response curve notably varied.

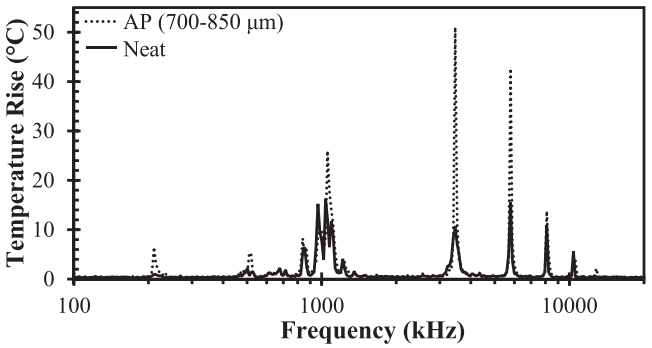

FIG. 4. Maximum temperature rise of the surface of the Neat and AP (700–850 μm) loaded samples versus frequency. Data is presented for 10 W of supplied electrical power at 2 s of excitation. Note the multiple common frequencies of interest.

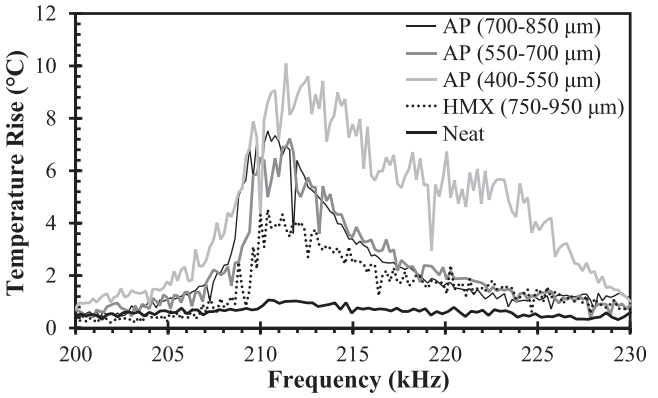

FIG. 5. Maximum temperature rise of the surface of the energetic particle samples versus frequency. Data is presented for 10 W of supplied electrical power at 2 s of excitation. Note that all of the samples exhibit clear resonant behavior in the vicinity of the listed transducer resonant frequency, and that the absolute level of temperature rise varies significantly.

To examine the variation near the transducer center frequency, the maximum surface temperatures observed at 2 s of excitation for energetic and inert samples excited between 200 to 230 kHz are shown in Figures 5 and 6, respectively. The thermal responses for all of the samples exhibit a local maximum between 205 and 220 kHz and the variation of the thermal responses highlights the effects of the various particle inclusions. The maximum surface temperature rises for all energetic samples, as well as the sugar (450–600 μm) and zirconium silicate (800–1000 μm) loaded samples, were on the order of 4 to 10 °C. All other inert samples result in a maximum surface temperature rise of 2 °C or less. The thermal results of the various particle sizes of the AP and zirconium silicate samples suggest that the magnitude of heating observed in this frequency region is not highly dependent on the size or mass of the inclusion.

The surface-averaged mechanical frequency response estimates for the AP (700–850 μm) loaded sample, neat sample and the transducer are shown in Figure 7. The mechanical surface responses were similar for all samples and closely reflect the thermal frequency response behavior observed in the maximum temperature rises as shown in Figure 4. This result illustrates that both the thermal and

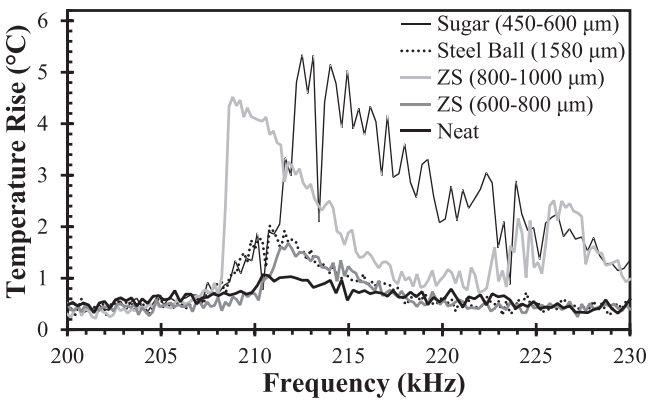

FIG. 6. Maximum temperature rise of the surface of the inert particle samples versus frequency. Data is presented for 10 W of supplied electrical power at 2 s of excitation. Note that all of the samples exhibit clear resonant behavior in the vicinity of the listed transducer resonant frequency.

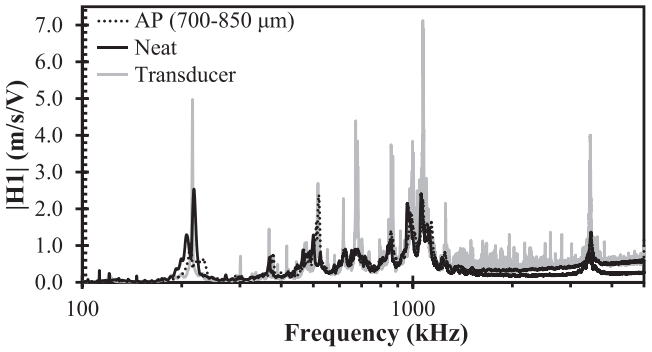

FIG. 7. Steady-state mechanical frequency response estimators of the Neat and AP (700–850 μm) loaded samples versus frequency at 0.130 W of excitation. Note the significant similarities between the responses, which suggest the mechanical response of the system is dominated by the transducer.

mechanical responses of the samples are extremely limited except at select frequencies.

A thermal image of the AP (700–850 μm) loaded sample surface after 2 s of excitation at 210.39 kHz and the root mean square (RMS) surface velocity of the sample at 210.25 kHz are shown in Figure 8. The thermal image of the sample surface shows localized heating in a pattern that closely reflects the physical locations of the particles highlighted in Figure 2. Thermal imaging of all of the samples, except the zirconium silicate and neat samples, illustrate localized heating at the particle locations in the frequency region near 215 kHz. The average surface velocity map of the sample illustrates that bulk motion of the sample surface occurs in this frequency region; however, there exists little spatial correlation with either the heating pattern of the sample surface or the particle locations. These results indicate that the source of heating is not linked to the near-surface motion of the sample, but is likely caused by local processes at the particle locations beneath the sample surface. As evident in Figure 8, variations of heating exist between the individual particles within each sample. This result may be due to unique surface features of each particle, allowing for variations in stress concentrations.

The thermal image of the AP (700–850 μm) loaded sample surface after 2 s of excitation at 983.45 kHz and the RMS surface velocity of the sample at 999.90 kHz are shown in Figure 9. The thermal image of the sample surface shows areas of localized heating; however, the thermal pattern does not correspond to the particle locations highlighted in Figure 2. The normalized surface velocity map of the sample shows concentrated areas of high surface motion in a spatial pattern similar to that observed in the thermal image. These results indicate that the observed heating in this frequency region is likely due to viscoelastic dissipation originating from the surface motion of the sample. This result reflects similar trends observed in all other samples in this frequency region and at higher frequency peaks. Complex heating patterns were also observed at certain frequencies between the

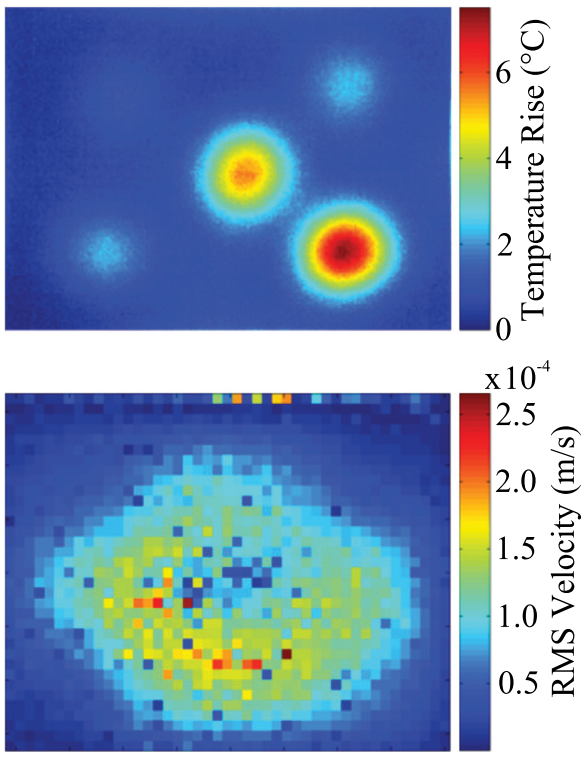

FIG. 8. Top: Thermal image representing the temperature rise of the surface of the AP (700–850 μm) loaded sample. Thermal data is presented for 10 W of supplied electrical power at 2 s of excitation at a frequency of 210.39 kHz. Bottom: RMS surface velocity map of the AP (700–850 μm) loaded sample. Surface velocity data is presented for 0.13 W of supplied electrical power at a frequency of 210.25 kHz. Note the overall lack of spatial similarity between the two data sets.

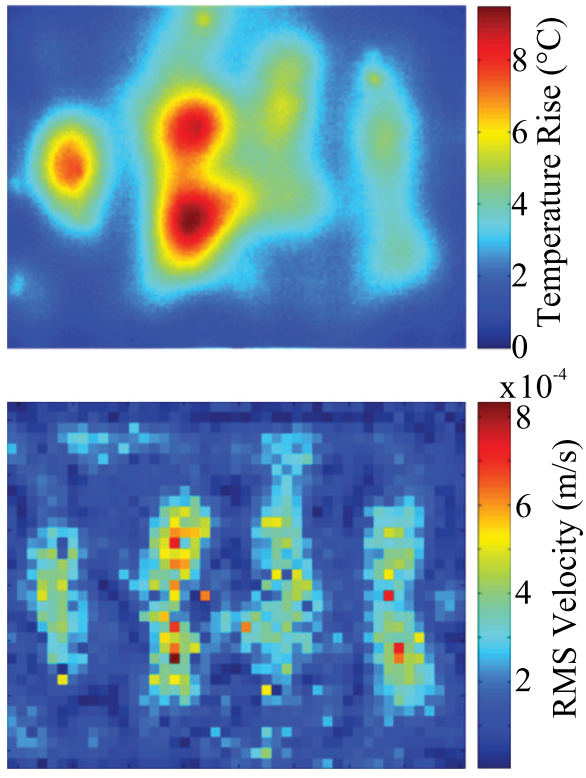

FIG. 9. Top: Thermal image representing the temperature rise of the surface of the AP (700–850 μm) loaded sample. Thermal data is presented for 10 W of supplied electrical power at 2 s of excitation at a frequency of 983.45 kHz. Bottom: RMS surface velocity map of the AP (700–850 μm) loaded sample. Surface velocity data is presented for 0.13 W of supplied electrical power at a frequency of 999.90 kHz. Note the similarity between the two sets of data, which is suggestive of viscoelastic heating.

215 kHz and 1 MHz regions. Patterns in this frequency region reflected both localized particle heating as well as heating due to broader viscoelastic dissipation as observed in the 215 kHz and 1 MHz regions, separately.

The time histories of the maximum temperatures located within the area of highest localized heating of the AP (700–850 μm) loaded sample excited at 210.39 and 983.45 kHz are shown in Figure 10. At the excitation frequency of 210.39 kHz, no significant temperature rise is observed on the surface of the sample until after approximately 0.75 s of excitation, which is indicative of the time required for heat to diffuse from the source to the sample surface. The heating observed in this frequency region is therefore likely due to processes occurring at the inclusion. This result is typical for excitation frequencies near the listed transducer resonance of 215 kHz for all of the samples except for the zirconium silicate and neat samples. Conversely, the near immediate temperature rise at the excitation frequency of 983.45 kHz indicates that the heat source is near the sample surface and is likely due to the viscoelastic heating produced by the surface motions observed in this frequency region. The immediate temperature rise was typical at excitation frequencies at or above 1 MHz for all samples.

The temperature distribution resulting from a point heat source of constant strength in an infinite medium is given by[15]

$$T(r,t) = \frac{q}{4\pi kr}\,\mathrm{erfc}\left(\frac{r}{\sqrt{4\alpha t}}\right), \tag{1}$$

where T is the local temperature, q is the constant heat generation rate of the point source, k is the thermal conductivity of the medium, r is the distance away from the point source, erfc is the complimentary error function, α is the thermal diffusivity of the medium, and t is time. An insulated boundary condition to simulate the sample surface may be realized by applying the method of images to the constant strength point source solution[15] to yield a semi-infinite solution for the local surface temperature directly above the point source

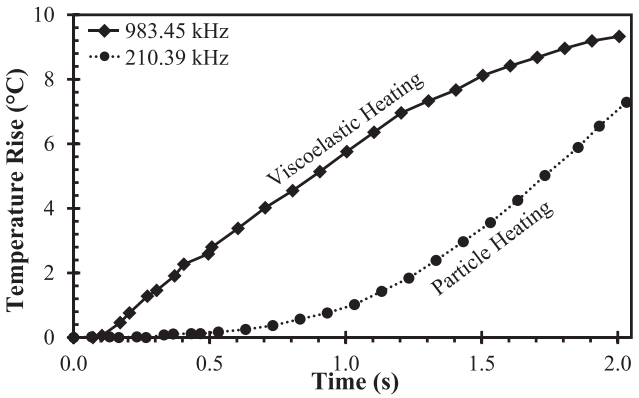

FIG. 10. Time histories of the maximum temperatures located within the area of highest localized heating of the AP (700–850 μm) loaded sample. Data is presented for 10 W of supplied electrical power at two frequencies illustrating different mechanisms of heat generation. The viscoelastic curve features an immediately observable temperature increase, while particle-based heating exhibits the effects of a finite time of heat diffusion through the binder.

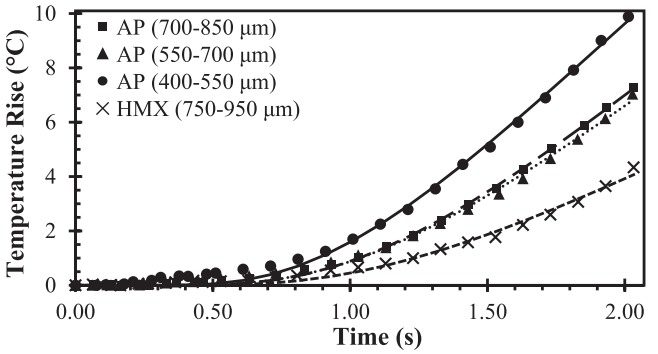

FIG. 11. Time histories of the maximum temperatures located within the area of highest localized heating of the energetic particle samples. Data is presented for 10 W of supplied electrical power at frequencies near 215 kHz. Continuous lines represent the temperature solutions to the corresponding fitted 1-D transient heat source models.

$$T_s(t) = \frac{q}{2\pi kd}\,\mathrm{erfc}\left(\frac{d}{\sqrt{4\alpha t}}\right), \tag{2}$$

where T_s is the local surface temperature directly above the point source and d is the depth of the source beneath the surface.

This analytical solution was fit to the measured maximum surface temperature histories near the 215 kHz peak for each sample by solving for the source depth, d, and the constant heat generation rate of the point source, q, using a simple least-squares method. Values of 1.382×10^{-3} cm^2/s and 0.232 W/m-K were used for the thermal diffusivity and conductivity of Sylgard 184, respectively.[16] The surface temperature histories within the area of highest concentrated heating are shown for each of the energetic and inert samples in Figures 11 and 12, respectively, along with the corresponding best-fit analytic solutions. The estimated heat generation rate and source depth at the selected excitation frequency for each sample are listed in Table II, as well the physical depths of the embedded particles. All of the temperature histories demonstrate similar trends indicating a heat diffusion time on the order of approximately 0.75 s, except for the zirconium silicate (800–1000 μm) and zirconium silicate (600–800 μm) loaded samples. The temperature histories of the zirconium silicate samples illustrate a near

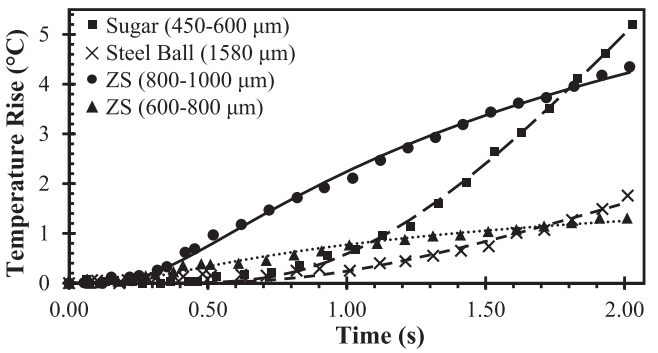

FIG. 12. Time histories of the maximum temperatures located within the area of highest localized heating of the inert particle samples. Data is presented for 10 W of supplied electrical power at frequencies near 215 kHz. Continuous lines represent the temperature solutions to the corresponding fitted 1-D transient heat source models.

TABLE II. Estimated heat generation rates and point source depths recovered from periodic excitation at frequencies near 215 kHz.

Sample description	Frequency (kHz)	Particle depth boundary (mm)	Heat source depth (d) (mm)	Heat generation (q) (W)
AP (700–850 μm)	210.39	0.91–1.69	1.41	0.250
AP (550–700 μm)	211.58	1.17–1.80	1.39	0.221
AP (400–550 μm)	211.38	1.06–1.54	1.31	0.231
HMX (750–950 μm)	210.39	1.14–1.99	1.45	0.162
Sugar (450–600 μm)	212.52	1.01–1.54	1.44	0.200
Steel Ball (1580 μm)	210.79	1.11–2.69	1.35	0.045
ZS (800–1000 μm)	208.82	1.05–1.95	0.69	0.012
ZS (600–800 μm)	211.78	1.19–1.89	0.58	0.002

immediate temperature rise, similar to the trends in the frequency region at or above 1 MHz. This result agrees with the absence of heating patterns corresponding to the particle locations observed for the zirconium silicate samples.

Although the analytical solution describes a point heat source of constant strength in an insulated semi-infinite medium, the solution works well to describe the observed surface temperature histories of all the samples in the frequency region near the listed transducer resonance. The estimated heat generation rates are significantly higher in the AP, HMX, and sugar samples than in the steel ball and zirconium silicate samples. Due to the highly repeatable nature of the experiment, significant heating caused by chemical reactions of the AP and HMX particles are unlikely. The higher heating rates for the AP, HMX, and sugar particle samples may be linked to microscale features on the surfaces of the energetic and sugar particles, as shown in Figure 1. The surface asperities of these particles may enable localized frictional heating, whereas the comparatively smooth surfaces of the steel ball and zirconium silicate particles may limit this process.

The estimated heat source depth directly corresponds with the physical depth of the embedded particles for all of the samples except for the zirconium silicate (800–1000 μm) and zirconium silicate (600–800 μm) loaded samples. This result again indicates that the major heating processes for all of the samples, except for the zirconium silicate samples, are located at the particle inclusions. The heating processes for the zirconium silicate samples in this frequency region are located near the sample surface and are likely viscoelastic in nature.

The analytical solutions for each sample were evaluated at a distance of the average particle radius in order to estimate the temperature rise near the particle surface. The estimated particle surface temperatures at peak frequencies near the transducer resonance are listed in Table III and are compared to the maximum sample surface temperatures observed at frequencies near or above 1 MHz. The estimated particle surface temperatures indicate that very high temperature rises are experienced at the AP, HMX, and sugar particles and that more mild temperature rises occur for the steel ball and zirconium silicate particles.

The estimated temperatures indicate that chemical decomposition of the AP (450 °C[17]) and HMX (253 °C[18]) particles may occur under higher power or longer excitation time. During separate thermal trials, conducted at heightened excitation parameters, the center crystal of the AP (550–700 μm) loaded sample was driven to decomposition within 10 s at an excitation level of 10 W at 215.00 kHz. Select frames from the high-speed optical imaging of this event are shown in Figure 13. Additionally, the center crystal of the HMX (750–950 μm) loaded sample was driven to decomposition within 15 s at an elevated excitation level of 16 W at 210.00 kHz. Additional AP and HMX samples were excited at similar parameters and only some produced evidence of decomposition, possibly indicating the importance of particle surface asperities to the generation of frictional heating.

TABLE III. Estimated particle temperatures and experimental maximum surface temperatures at 2 s of excitation.

	Particle heating		Viscoelastic heating	
Sample description	Frequency (kHz)	Est. particle surface temp. rise (°C)	Frequency (kHz)	Max. surface temp. rise (°C)
AP (700–850 μm)	210.39	133.42	3460.60	50.66
AP (550–700 μm)	211.58	163.54	1055.69	61.78
AP (400–550 μm)	211.38	250.58	5785.32	72.87
HMX (750–950 μm)	210.39	74.24	1055.69	57.93
Sugar (450–600 μm)	212.52	189.07	1055.69	35.87
Steel ball (1580 μm)	210.79	5.67	3399.81	24.20
ZS (800–1000 μm)	208.82	5.96	1074.56	38.93
ZS (600–800 μm)	211.78	1.82	1055.69	62.25

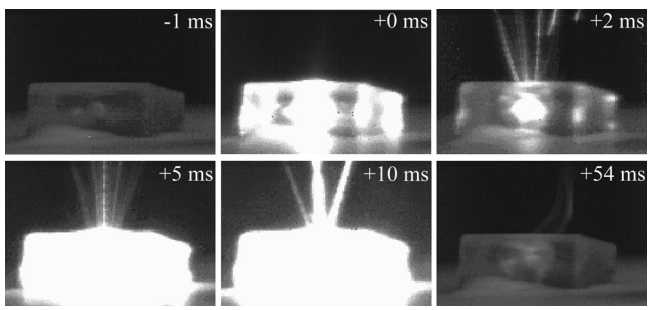

FIG. 13. Select frames from the high speed optical imaging of the explosive decomposition of the AP (550–700 μm) loaded sample. Ignition was observed for 10 W of electrical excitation at 215 kHz. Time markers are with respect to first light from ignition. Note that a void created from the event is visible in the last frame.

IV. CONCLUSIONS

The thermal and mechanical responses of elastic binder samples with varied inert and energetic particle inclusions excited under high-frequency contact excitation are presented. Evidence of two major heating mechanisms, frictional heating located at the particle and viscoelastic heating located near the sample surface was observed. The magnitude and underlying mechanism of the thermal response depend on the frequency of excitation. At excitation frequencies near the listed transducer resonance of 215 kHz, the heating and surface velocity patterns indicate that the heat source was located at the particle location, except for the zirconium silicate samples. The heating mechanism in this frequency region is likely linked to frictional effects concentrated at microscale surface features on the particles. At select excitation frequencies near and above 1 MHz, the heating and surface velocity patterns indicate that the heating is closely linked to the surface motion, suggesting that the mechanism is likely due to viscoelastic heating near the sample surface.

An analytical solution for the temperature distribution in response to a point heat source of constant strength in an insulated semi-infinite medium was used to estimate the heating rate and source depth for each sample when excited near the listed transducer resonance frequency. The analytical solutions agreed well with the observed temperature histories for all samples and the estimated heat source depths correspond to the particle depths for all of the samples except for the zirconium silicate (800–1000 μm) and zirconium silicate (600–800 μm) loaded samples. The fitted analytical solutions were used to estimate the temperature rises experienced at the embedded particle surface. Under heightened excitation parameters, the center particles within the AP (550–700 μm) loaded sample and HMX (750–950 μm) loaded sample were driven to decomposition within 15 s of excitation. Additional energetic samples were mechanically excited under similar experimental conditions and some samples exhibited evidence of chemical decomposition.

High-frequency mechanical excitation has been shown to be an effective method of producing internal heat generation within a particle-binder system and can induce decomposition of individual particles of AP and HMX embedded within Sylgard 184. This process, when applied in composite explosives, may lead to an increase in detectability, and potentially an alternative method for defeat. Future work should investigate the significance of the surface roughness of the embedded particles, as well as the effects of varying the stiffness and adhesion of the binder. Further studies should also investigate frictional heating due to particle-particle interactions in high-solids-loaded systems, which are more typical of realistic composite explosives.

ACKNOWLEDGMENTS

This research was supported by the U.S. Office of Naval Research under the Multidisciplinary University Research Initiative on "Sound and Electromagnetic Interacting Waves" through Grant No. N00014-10-1-0958 and under the Basic Research Challenge on "Chemical Decomposition in High Energy Density Materials Induced by Coupled Acoustic Electromagnetic Energy Insult" through Grant No. N00014-11-1-0466. J.O.M. also wishes to acknowledge the National Science Graduate Research Fellowship Program under Grant No. DGE-1333468.

[1]A. B. Bhatia, *Ultrasonic Absorption: an Introduction to the Theory of Sound Absorption and Dispersion in Gases, Liquids, and Solids* (Courier Dover Publications, 1967).
[2]M. N. Tolunay, P. R. Dawson, and K. K. Wang, Polym. Eng. Sci. **23**, 726 (1983).
[3]G. T. Haar and C. Coussios, Int. J. Hyperthermia **23**, 89 (2007).
[4]D. S. Moore, "Method and apparatus for detecting explosives," U.S. patent 7,939,803 (2011).
[5]D. S. Moore, Rev. Sci. Instrum. **75**, 2499 (2004).
[6]H. Ostmark, S. Wallin, and H. G. Ang, Propellants, Explosives, Pyrotechnics **37**, 12 (2012).
[7]N. Loginov, S. Muratov, and V. Epifanov, Combust. Explosion Shock Waves **25**, 58 (1989).
[8]J. Renshaw, J. C. Chen, S. D. Holland, and R. B. Thompson, NDT & E International **44**, 736 (2011).
[9]J. Renshaw, S. D. Holland, and D. J. Barnard, NDT & E Int. **42**, 753 (2009).
[10]C. Homma, M. Rothenfusser, J. Baumann, and R. Shannon, AIP Conf. Proc. **820**, 566 (2006).
[11]J. K. Miller and J. F. Rhoads, in *Proceedings of the 2013 ASME IDETC/CIE Conferences*, DETC2013-12138 (2013).
[12]D. C. Woods, J. K. Miller, and J. F. Rhoads, in *Proceedings of the 2014 ASME IDETC/CIE Conferences*, DETC2014-34516 (2014).
[13]J. O. Mares, J. K. Miller, N. D. Sharp, D. S. Moore, D. E. Adams, L. J. Groven, J. F. Rhoads, and S. F. Son, J. Appl. Phys. **113**, 084904 (2013).
[14]M.-W. Chen, S. You, K. S. Suslick, and D. D. Dlott, Rev. Sci. Instrum. **85**, 023705 (2014).
[15]H. Carslaw and J. Jaegar, *Conduction of Heat in Solids* (Clareden Press, 1959).
[16]G. L. Flowers, B. D. Faubion, J. L. Montague, and S. T. Switzer, "Selected physical and thermal properties of various formulations of silicone potting compounds," Technical Report, DTIC Document #ADA302639, 1980.
[17]A. G. Keenan and R. F. Siegmund, Q. Rev. Chem. Soc. **23**, 430 (1969).
[18]T. R. Gibbs and A. Popolato, *LASL Explosive Property Data* (University of California Press, 1980), Vol. 4.